




# Synthesis of Zn-doped lead sulphide by electrodeposition: potential change on structural, morphological, and optical properties

Erman Erdoğan<sup>1,\*</sup>  and Ayca Kiyak Yildirim<sup>2</sup>

<sup>1</sup>Electronic Communication Technology Program, Vocational High School, Bilecik Seyh Edebali University, 11100 Bilecik, Turkey

<sup>2</sup>Department of Opticianry, Health Services Vocational School, Bilecik Seyh Edebali University, 11100 Bilecik, Turkey

**Received:** 17 November 2022

**Accepted:** 18 March 2023

**Published online:**  
3 April 2023

© The Author(s), under exclusive licence to Springer Science+Business Media, LLC, part of Springer Nature 2023

## ABSTRACT

PbS and Zn-doped PbS materials, which have many fields of study, stand out with their applications in electro-optic technology. In this study, pure, 2%, and 4% Zn-doped PbS films annealed at 250 °C annealing temperature were produced on Indium Tin Oxide substrates by electrodeposition method. Structural, optical, and morphological properties of these produced films were examined by broad range analysis methods, and the effect of Zn element doped for various rates on the films was reported. From the structural features of the films specified by X-ray diffraction, it was concluded that all of the films were in polycrystalline structure. The thickness of the films and the parameters defining some optical properties (extinction coefficient and refractive index) were stated by spectroscopic ellipsometer. The thickness values ranged between 245 and 232 nm. According to the measurements determined by the optical method, it was found that the optical band gaps of all the films were between 1.95 eV and 2.07 eV. The transmittance values of the films at the visible wavelength (400–700 nm) were determined as low. The surface morphologies and elemental analyses of the films were obtained by Scanning Electron Microscopy and Energy-Dispersive X-ray Spectroscopy, respectively. As a result of the investigations, it was concluded that the Zn dopant had a healing effect on the structural, optical, and surface properties of the films.

## 1 Introduction

Progress in science and technology are very important for the development of new materials. Innovations and discoveries in the field of materials focus on the production of high-quality materials. Among

parameters that determine material properties and performance are not only the composition, but also the control of structure and/or microstructure with appropriate production methods. The importance of semiconductors in technological applications is quite large. Advances in electronics and computer

Address correspondence to E-mail: erman.erdogan@bilecik.edu.tr

technology have been possible with better knowledge of the properties of semiconductors, and thus technological developments have accelerated [1]. Thin films are used as high-tech materials in industries related to optics, electronics, magnetics, chemicals, and mechanics because they add many properties that they cannot provide alone when coated on the surface of bulky materials. In addition, they can be used as electronic circuit elements, since they behave like new materials, and they are completely different from their volume properties, produced in multilayers [2]. Semiconductor thin films, which have an important place in today's science and technology, can be produced with various techniques. The physical properties of thin films such as structural, morphological, optical, electrical, and magnetic properties are of great importance in determining the usage areas of thin films. For this reason, it is important to examine the structural, surface, optical, and electrical properties of thin films in detail and the experimental methods used for this [3, 4].

Lead Sulfide (PbS), which can be used as an absorber layer in solar cells, is in the IV–VI semiconductor group [5]. Studies have shown that PbS responds much more to temperature and band gap changes compared to other IV–VI semiconductors [6]. It is also highly sensitive to grain size compared to other semiconductors such as Si. These properties have led to the widespread use of PbS in the production of nanostructured devices. PbS semiconductor films can be prepared by many methods. Microwave heating [7], SILAR [8], sputtering [9], spray pyrolysis [10], and chemical bath deposition [11] methods are some of the methods used in the production of PbS films.

Most of the aforementioned methods are not suitable for large surface coatings, low-temperature process, and low production cost. In addition, the materials to be used to cover large areas are quite expensive. Electrodeposition method, which will be used in this study, is an interesting method for thin film production because it is low cost and easy to implement. By this method, films can be deposited at the desired density and thickness by controlling the electric field, pH, and deposition times. It also has important advantages such as easy control of film parameters and being applicable in room conditions without the need for any complex experimental setup [12, 13].

Doping plays an important role in obtaining quality semiconductor materials. It is generally effective in controlling the grain size, surface morphology, and crystal structure [14]. For this reason, it is possible to change the structural, optical, electrical, and magnetic characteristics of PbS thin films through doping with miscellaneous elements. There are various reports on PbS thin films doped with distinctive elements [15–18], however, choosing the appropriate doping elements and the best ratio to get high-quality PbS thin films is still a challenge for researchers.

In this study, zinc was chosen as an additive to optimize the optoelectronic characteristics of PbS thin films. We prosperously designed pure and Zn-doped PbS films on ITO substrates using electrochemical deposition, then investigated how Zn doping concentration affects the microstructural, morphological, and especially optical properties of PbS thin films. When compared with some physical properties of Zn-doped PbS thin films obtained in literature survey, obtaining results by using a simple, cheap, useful method that does not require a vacuum environment, spectroscopic ellipsometer analysis, and finding dispersion parameters reveal the importance and novelty of this study.

## 2 Experimental

All chemical reagents we purchased were of analytical quality and were used without further purification. Optically transparent ITO-coated glasses with a surface area of  $1.65 \text{ cm}^2$ , a resistance of  $25 \Omega / \text{cm}^2$ , and a thickness of 100 nm were used to produce PbS semiconductor films. ITO-coated glasses were first soaked in deionized water (DI). After being kept in isopropyl alcohol solution for 10 min, it was rinsed in DI water. Rinsed ITO-coated glasses were dried at room temperature ( $25 \text{ }^\circ\text{C}$ ) for 30 min so that no moisture remained on the surface.

In the solution preparation steps for PbS compound,  $\text{Pb}(\text{NO}_3)_2$  as Pb source,  $\text{Na}_2\text{S}_2\text{O}_3$  as S source, ethylenediaminetetraacetic acid (EDTA) as reaction accelerator, and potassium chloride (KCl) as supporting electrolyte were used. In the solution preparation steps for Zn dopant, zinc nitrate hexahydrate ( $\text{Zn}(\text{NO}_3)_2 \cdot 6\text{H}_2\text{O}$ ) was used. DI water was used as solvent in film production. In order to avoid pH difference, the solutions were first prepared as 1 L and production was carried out by taking 100 mL

from each. 0.01 M  $(\text{NO}_3)_2$ , 0.05 M  $\text{Na}_2\text{S}_2\text{O}_3$ , and 1 L of DI water were poured into a vessel to prepare an aqueous solution of 0.0025 M EDTA and 0.1 M KCl. After these compounds were added, they were mixed with a magnetic stirrer for 1 h. The solution pH value was adjusted to 2.5 for all mixtures. The production of PbS films by electrochemical deposition method was carried out with a three-electrode IVIUM VERTEX Potentiostat/Galvanostat device which served as DC supply unit and was set at a constant voltage of 1.8 V for 100 s.

While performing the electrochemical deposition process, Ag/AgCl reference Electrode was used. The standard potential of the selected reference electrode is 0.222 V at 25 °C. Platinum flat wire was used as the counter electrode. ITO-coated glass substrates prepared as working electrodes were used. During film production, WiseStir brand MSH-20D model electronic magnetic stirrer and heater were used to mix and heat the solutions. All deposited thin films were annealed at 250 °C for 5 min.

The surface formations of pure 2% and 4% Zn-doped PbS thin films deposited on the ITO-coated substrate were examined by scanning with the ZEISS Supra 40 VP electron microscope (SEM). The percentages of atomic components of these thin films were determined by the energy-dispersive X-ray (EDX) system. X-ray system with  $\text{CuK}\alpha$  radiation ( $\lambda K\alpha = 1542 \text{ \AA}$ ) was used to detect the crystal structure of the materials (Panalytical Empyrean). Optical absorption and reflection spectra were measured using UV-Vis spectrometer. All of these measurements were carried out at Bilecik Seyh Edebali University Central Research Laboratory. Film thickness, refractive indices, and extinction coefficient were determined using a spectroscopic ellipsometer device. These measurements were carried out in Niğde Ömer Halisdemir University Central Laboratory. With the aid of a spectroscopic ellipsometer, the thicknesses of pure, 2%, and 4% Zn-doped PbS thin films were determined as 245 nm, 238 nm, and 232 nm, respectively.

### 3 Results and discussions

#### 3.1 XRD investigations

X-ray diffraction patterns were performed to analyze the structural properties of the deposited pure and

Zn-doped PbS thin films at different rates. By comparing the obtained diffraction patterns with the reference JCPDS (Joint Committee on Powder Diffraction Standards) cards, the miller indices of the peaks seen on the pattern and their crystal systems were determined. XRD patterns of PbS:Zn films are given in Fig. 1.

The presence of more than one peak in the diffraction patterns given in Fig. 1 indicates that the deposited films have a polycrystalline structure. It was determined that the XRD patterns of all the deposited films were in good agreement with JCPDS Card No: 98-006-8701. The results showed that the samples had a orthorhombic structure and were free of for pure PbS structure to other impurities. However, minor impurities were present at 2% and 4% Zn-doped structures and at  $2\theta$  angles of 21.29° and 48.63°. Similar observation was reported for Ag-doped PbS structures by M.H. Jameel and his friends [19]. The XRD patterns indicate that the two high-intensity peaks corresponding to the (102) at  $2\theta$  angles of 28.66° and (104) at  $2\theta$  angles of 31.78° planes and the low-intensity peak corresponding to (008) at  $2\theta$  angles of 37.17° belong to the ZnS structure [20]. Full width half maximum (FWHM) values changed with the increase of Zn content of thin film samples. This change is related to the change in grain size. The grain sizes of thin film samples are calculated with the modified Scherrer plot according to the following formula [21, 22]:

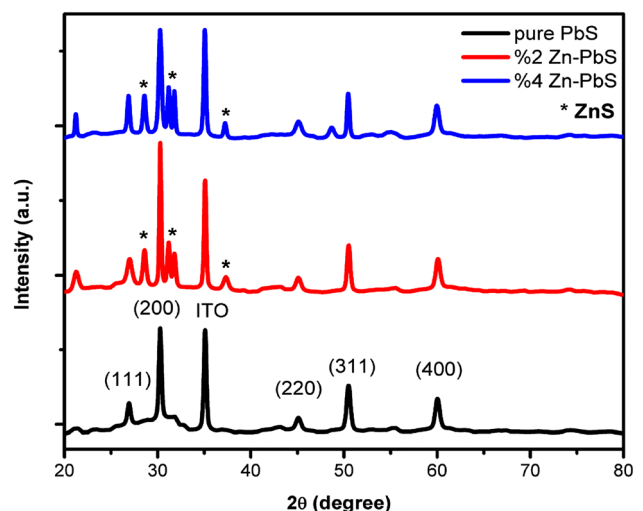


**Fig. 1** XRD graph of pure, 2%, and 4% Zn-doped PbS thin film samples

$$\ln \beta = \ln \frac{0.9\lambda}{D} + \ln \frac{1}{\cos \theta}, \quad (1)$$

where “ $D$ ” is the size of crystal, “ $\lambda$ ” is of the incident X-ray wavelength (1.542 Å),  $\beta$  is the full width half maximum, and  $\theta$  is the angle of the X-ray diffraction peaks. If we plot the data for  $\ln \beta$  with respect to  $\ln (1/\cos \theta)$ , a slope with line and a crossing of  $\ln 0.9\lambda/D$  should be existed. Consequently, a single nanometer-sized  $D$  value can be calculated. In view of the computed average size of crystal values of the examples from the intersection point of the graph given in Fig. 2, Table 1, it was comprehended that the size of crystal changed with increasing Zn amount. The change in size of crystallite of Zn-doped PbS may be due to the replacement of smaller zinc ions instead of large lead ions, because the atomic radius of the lead atom (1.21 Å) is greater than that of the zinc atom (0.74 Å). Similar observation is reported for Zn-doped PbS thin films for reference number of [23]. The lattice parameters ( $a$ ,  $b$ , and  $c$ ) are computed via the following relation:

$$\frac{1}{d_{hkl}^2} = \frac{h^2}{a^2} + \frac{k^2}{b^2} + \frac{l^2}{c^2}, \quad (2)$$

where  $d_{hkl}$  is the distance between planes,  $\lambda$  is the wavelength of the X-ray source, and  $\theta$  is the diffraction angle. The volume of the crystal is also computed by multiplying the lattice parameters. Table 1 demonstrates the obtained data. As the amount of dopant increases, the lattice parameters and volume of the structure also change. The reason for this

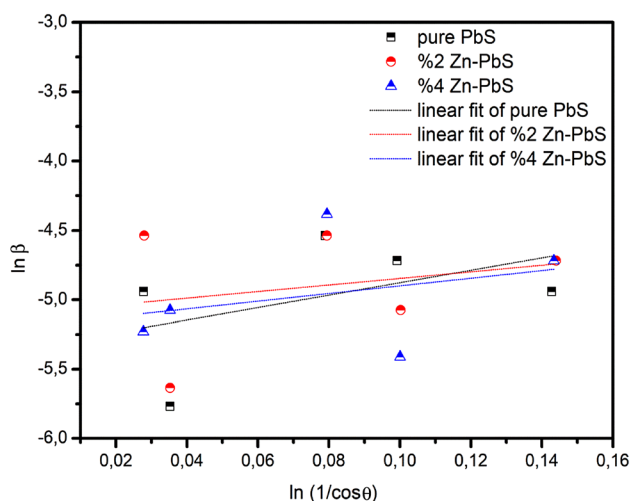


**Fig. 2** Scherrer plots of pure, 2%, and 4% Zn-doped PbS thin film samples

change in the lattice parameters is the displacement of the Pb cation and Zn cations of any doped PbS compound into the lattice, the oxidation–reduction reactions in the doping cations that occur during the displacement, and the difference in the effective ion radii between the displaced cations.

### 3.2 SEM investigations

The morphological properties of a material obtained in the form of a semiconductor film should be analyzed in detail. One of the most common techniques used for this is scanning electron microscopy (SEM).

Morphological examinations of pure, 2%, and 4% Zn-doped PbS thin film samples were obtained by taking surface images by SEM. The elemental composition of the produced samples was determined using EDX (Energy-dispersive X-ray spectroscopy) integrated into the SEM device. SEM graphs of pure, 2%, and 4% Zn-doped PbS thin films are given in Fig. 3.

When the SEM images of the pure, 2%, and 4% Zn-doped PbS thin films in Fig. 3 were examined, it was observed that the film was homogeneously distributed on the surface and covered every part of the surface without forming agglomerations. E. A. Abiodun et al. deposited nanostructured PbS and Zn-doped PbS thin films and they reported that the deposited films appear to form regularly, and the shaped crystallites and particles were evenly distributed across the substrate surface [24]. No deterioration was observed in terms of homogeneity on the surface of the PbS thin films produced due to the increasing Zn dopant ratio.

EDX graphs of pure, 2%, and 4% Zn-doped PbS thin films are shown in Fig. 4. When EDX graphs are examined, it is seen that mainly lead and sulfur are present. In the EDX graphs of 2%, and 4% Zn-doped PbS thin films, it is seen that there are 2.42% and 3.37% Zn elements atomically, respectively, and these results are also given in Fig. 4. These results are proof that the Zn element enters the PbS thin film structure. M. A. Hussain et al. had similar observation in their study [25].

The fact that sulfur element has a lower melting point compared to lead element, and therefore evaporation of sulfur from the film surface may be possible, this situation can be attributed to the presence of different and small amounts of sulfur element in EDX results [26].

**Table 1** Various parameters from structural examination ( $d_{hkl}$ : interplanar distance, FWHM: full width half maximum,  $D_{SR-ort}$ : size of crystal obtained from plot, a, b, and c are the lattice parameters, V: volume of crystal

	(hkl)	$d_{hkl}$ (Å)	a (Å)	b (Å)	c (Å)	V (pm <sup>3</sup> )	2θ (°)	FWHM(°)	$D_{SR-ort}$ (nm)
Pure PbS	(111)	3.3147	11.90	5.83	5.80	402.80	26.09	0.4093	28
	(200)	2.9558					30.24	0.1791	
	(220)	2.0168					44.95	0.6140	
	(311)	1.8175					50.20	0.5117	
	(400)	1.5469					59.79	0.4093	
%2 Zn-PbS	(111)	3.3063	11.28	3.98	4.21	189.01	26.97	0.6140	22
	(200)	2.9548					30.25	0.2047	
	(220)	2.0117					45.07	0.6140	
	(311)	1.8091					50.45	0.3582	
	(400)	1.5413					60.03	0.5117	
%4 Zn-PbS	(111)	3.3208	12.88	4.34	4.42	247.07	26.85	0.3070	24

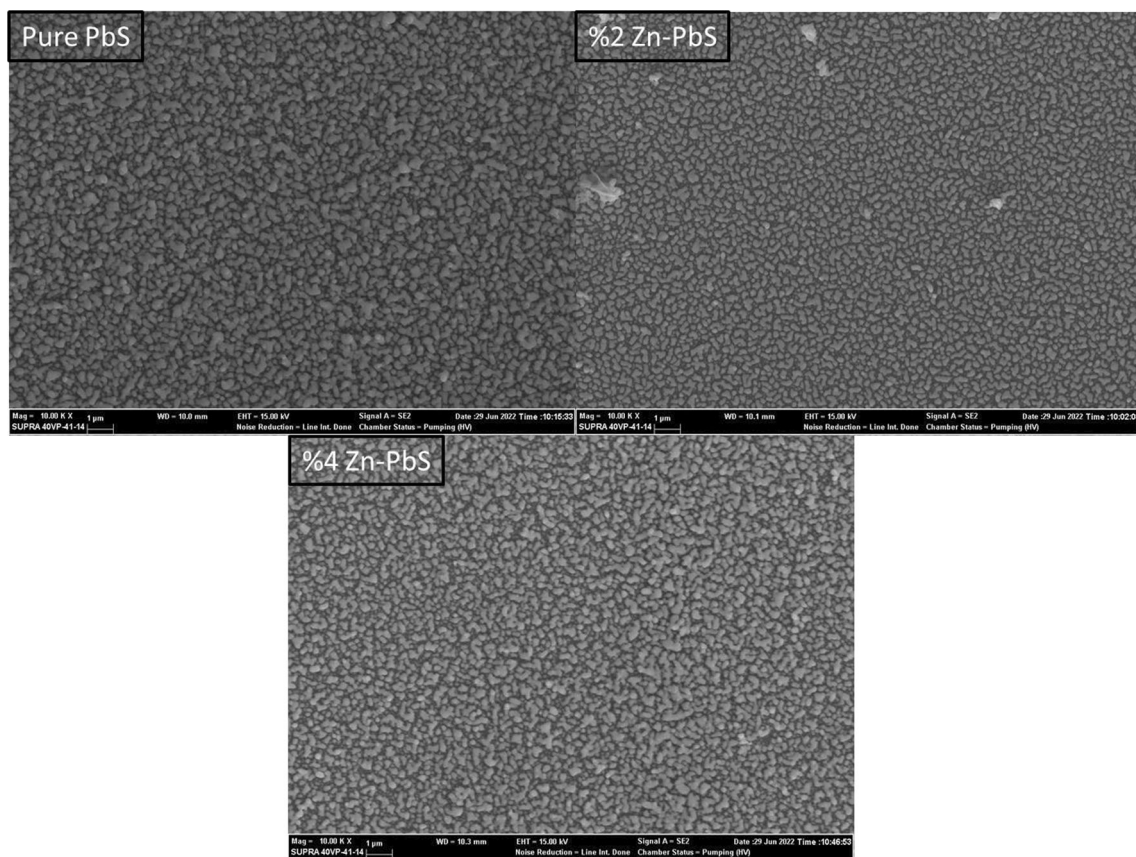


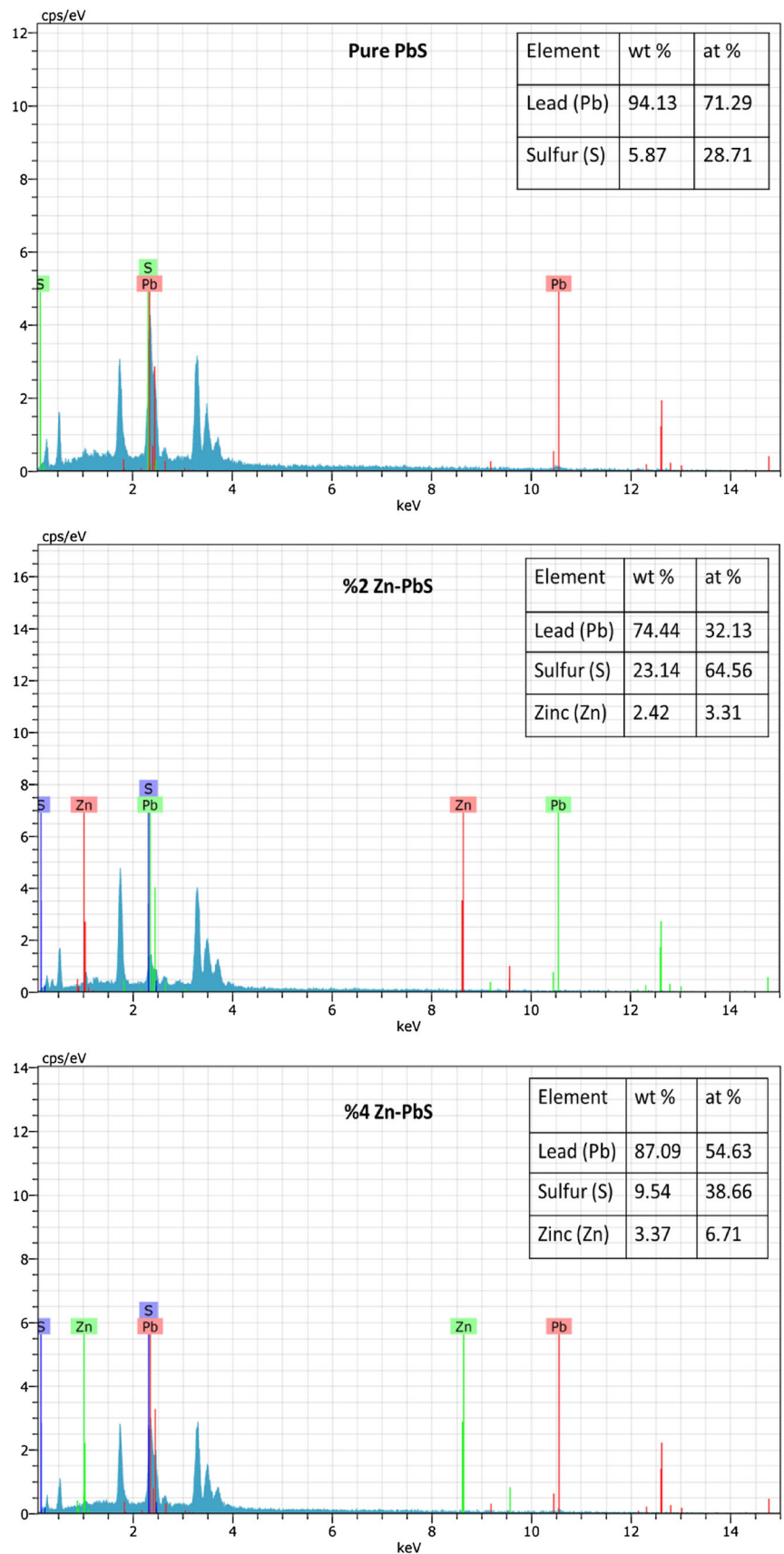
**Fig. 3** SEM images of pure, 2%, and 4% Zn-doped PbS thin film samples

### 3.3 Optical investigations

In order to survey the optical features of pure PbS, 2%, and 4% Zn-doped PbS films, transmittance and absorption spectra were taken, optical energy gaps were determined. Transmittance and absorption spectra measurement were obtained at room temperature and in the wavelength range of 300 to 1100 nm, by a spectrophotometer device. The

thickness, refractive indices, and extinction coefficients of these films were determined with the aid of spectroscopic ellipsometer device and the change of refractive indices against wavelength and extinction coefficients against wavelength were investigated. Before the measurements were taken, ground correction was made and thus the radiation passing through the glass was normalized to 100%. In this way, the optical transmittance and absorption values

**Fig. 4** EDX graph and elemental compositions of pure, 2%, and 4% Zn-doped PbS thin film samples



to be read on the films are made independent of the substrate absorption [27]. Then, the fundamental optical constants of Zn-doped PbS thin films were computed using the data obtained from the spectrophotometer by the help of some relations.

The absorption spectra of un-doped, 2%, and 4% Zn-doped PbS thin films are given in Fig. 5. As seen from the absorption spectra, thin films exhibit high optical absorption in the visible region but the absorption increases as the wavelength decreases. In the visible region, it seems that the absorption decreases, inversely to the increase in the transmittance spectra. In addition, it seems that the absorption of photons with wavelengths greater than 700 nm in all thin films is quite low, and as a result, the absorption edge is clearly formed. From this, it can be said that deep and shallow trap levels with different energy levels localized within the optical energy gap may be more intense, and therefore, low energy absorptions may be more. As can be seen in Fig. 5, the absorption edges of the Zn-doped films are shifted towards lower wavelengths compared to the pure PbS films. The cause of this event may also be blue shift. Similar observation has been seen in the study conducted by E. Veena et al. [28].

In addition, when the absorption spectra of all the films were examined, it was observed that there were improvements and recovery in the band edges with the Zn dopant compared to the pure film. This may be due to the reduction of band sagging at the absorption edges with Zn dopant.

Optical transmittance spectra of un-doped, 2%, and 4% (wt.) Zn-doped PbS thin films, respectively, are

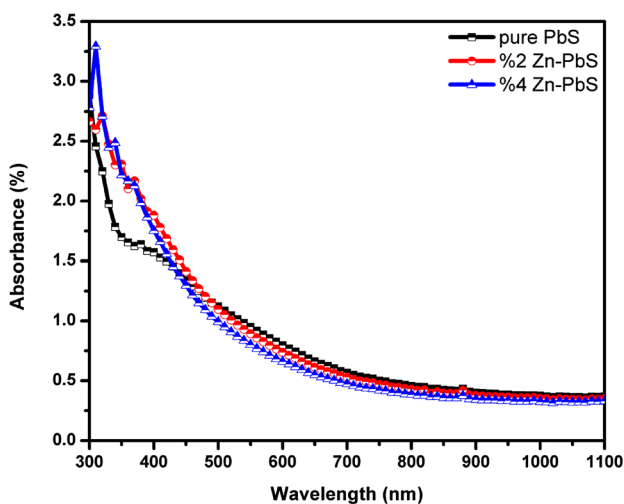


**Fig. 5** Absorbance graph of the PbS films with various Zn content

given in Fig. 6. When the figure was examined, it was observed that all Zn-doped thin film samples had better optical transmittance than the pure PbS sample. The highest optical transmittance was observed in PbS thin film sample with 4% Zn doped. Furthermore, it is seen that the optical transmittance values of PbS samples increase with the increase of Zn dopant ratio. M. Liu et al. examined the transmittance properties of PbS thin films and they found according to the transmittance spectrum that the value of transmittance of Zn-doped PbS films is higher than pure films [29]. As seen in Fig. 6, while each thin film exhibits very low transmittance in the visible region, it seems that the transmittance increases towards longer wavelengths. In addition, the improvement in the structural characteristics of the films with the increase in Zn dopant is effective on this increase in optical transmittance.

During the film formation, due to the inhomogeneity of the surface and its roughness, when the light falls on the surface of the film, the increase in optical scattering occurring on the surface causes a decrease in transmittance. Therefore, the Zn dopant may have increased the transmittance by reducing the optical scattering occurring on the surfaces or inner regions of the films. A. E. Adeoye et al. examined and revealed that pure PbS thin film has the lowest transmittance in the UV–Vis–NIR regions. The transmission of the films ordinarily rises with increasing Zn doping [30].

The optical band gaps of the films were determined by plotting the  $(\alpha h\nu)^2$  value against the photon

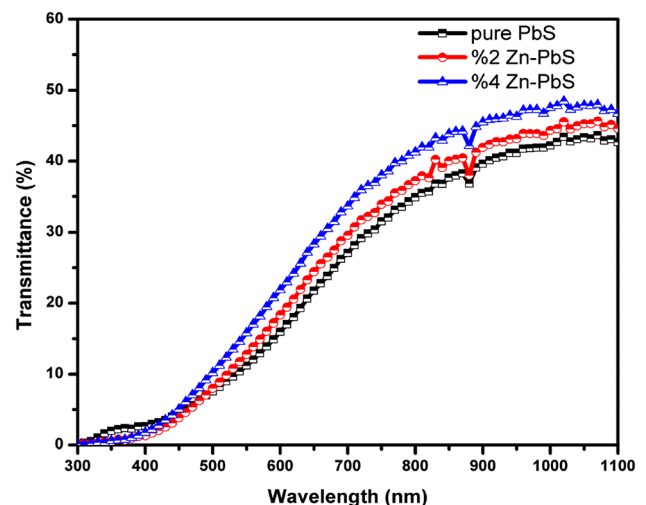


**Fig. 6** Transmittance graph of the PbS films with various Zn content

energy ( $h\nu$ ), using the thickness measured by the spectroscopic ellipsometer device and the absorption spectra measured by the UV–Vis spectroscopy [31].

Furthermore, the optical band gap of the pure PbS semiconductor thin films is calculated as 1.95 eV. Optical band gap values of 2 and 4% Zn-doped PbS semiconductor thin films were found to be 1.99 eV and 2.07 eV, respectively (see Fig. 7). S. Ravishankar and A.R. Balu reported that un-doped PbS film has a band gap of 2.12 eV, which is a higher value compared to that in this study. They also reported that the band gaps of 2%, and 4% Zn-doped PbS films were found to be 2.16 eV and 2.07 eV, respectively [32]. When the obtained data are examined, it is seen that the optical band gaps of the semiconductor thin films increase as the Zn doping ratio increases. This change is the expected effect of Zn addition to the thin film structure. It is seen that the band gap of the precipitated thin films is considerably higher than the band gap (0.41 eV) of the bulk PbS material.

When the studies in the literature are examined, it is stated that the optical band gap of PbS thin films consisting of nano-sized crystals is larger than the value in bulk form due to the quantum size effect, and the crystal size and the optical band gap change inversely [33, 34]. We think that the high optical band

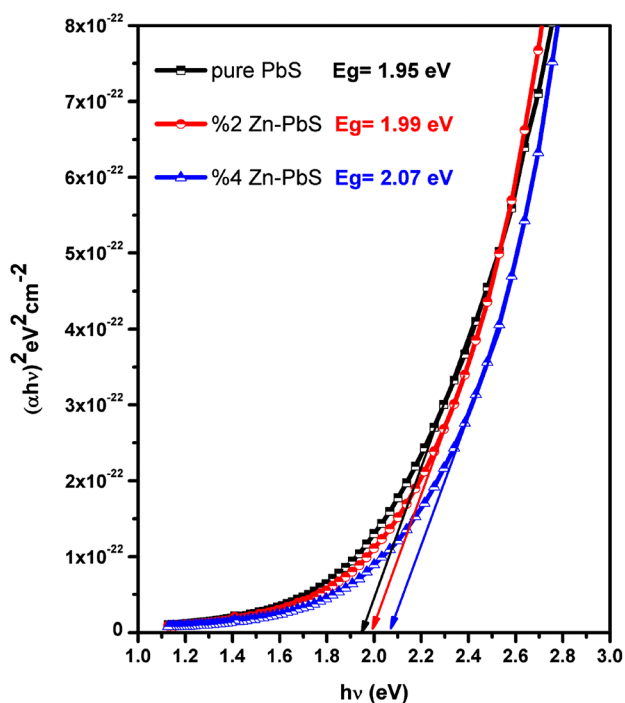


**Fig. 7** Changes of optical band gap values of PbS films with Zn content

gap values of polycrystalline PbS thin films precipitated in this study may be related to the crystal size of the thin films. However, considering that the precipitated thin films are formed in polycrystalline form, we think that the crystal size distributions should be taken into account to evaluate the change in the optical band gap range because the materials are composed of many crystals of different sizes in different orientations rather than uniform crystals [35].

### 3.4 Spectroscopic ellipsometry investigations

Spectroscopic ellipsometry is based on the principle of measuring the reflection effect of polarized light on the material. In spectroscopic ellipsometer measurements,  $\psi$  and  $\Delta$  spectra are recorded at each wavelength and angle of incidence. The  $\psi$  and  $\Delta$  parameters depend on the fresnel coefficients and are the parameters related to the optical and structural properties of the sample and are expressed by the following equation [36]:

$$\rho = \tan\psi e^{i\Delta} = R_p/R_s. \quad (3)$$

In this equation,  $R_p$  and  $R_s$  are defined as the complex reflection coefficients of light polarized parallel ( $p$ ) and vertically ( $s$ ) to the plane of incidence, respectively.  $\Delta$  reflects the change in phase difference between incident and reflected waves for the  $p$ -polarized and  $s$ -polarized components.  $\tan\psi$  is expressed as the ratio of the reflection coefficient polarized parallel to the incident plane to the reflection coefficient polarized perpendicular to the incident plane, and  $\rho$  is defined as the complex reflectance ratio.

Incidence angle of light used for the measurements was  $70^\circ$ , for the measured spectral range of 300–1000 nm.  $\Delta$  and  $\psi$  values against wavelength of pure, 2%, and 4% Zn-doped PbS films are shown in Fig. 8a, b. As can be seen from this figure, there are deviations from the theoretical and experimental values in the spectra. The MSE values of pure, 2%, and 4% Zn-doped PbS films are found to be 2919, 2729, and 2644, respectively. The MSE values both  $\Delta$  and  $\psi$  for  $\text{HfO}_2$  films were found to be smaller than our values, which is about 1.42 for reference of [37]. It is thought that the factors affecting these deviations are due to the method used in the coating, the surface



properties, and the grain boundaries of the films and the reflection of light from the glass substrates [38].

In order to design semiconductor devices properly, the dispersion of refractive indices should be investigated. Knowing the optical dispersion and other optical parameters of the material in device design is important for many integrated device studies where the refractive index is important, such as filters, switches, and modulators. The refractive index of an optical medium is quantity without dimension that defines the propagation of the beam through that medium. The refractive index determines how fast light passes through an object [39].

From Fig. 9 it is understood that the refractive indices values of pure and Zn-doped PbS thin films vary in the range of 0.6–1.8 in the visible region.

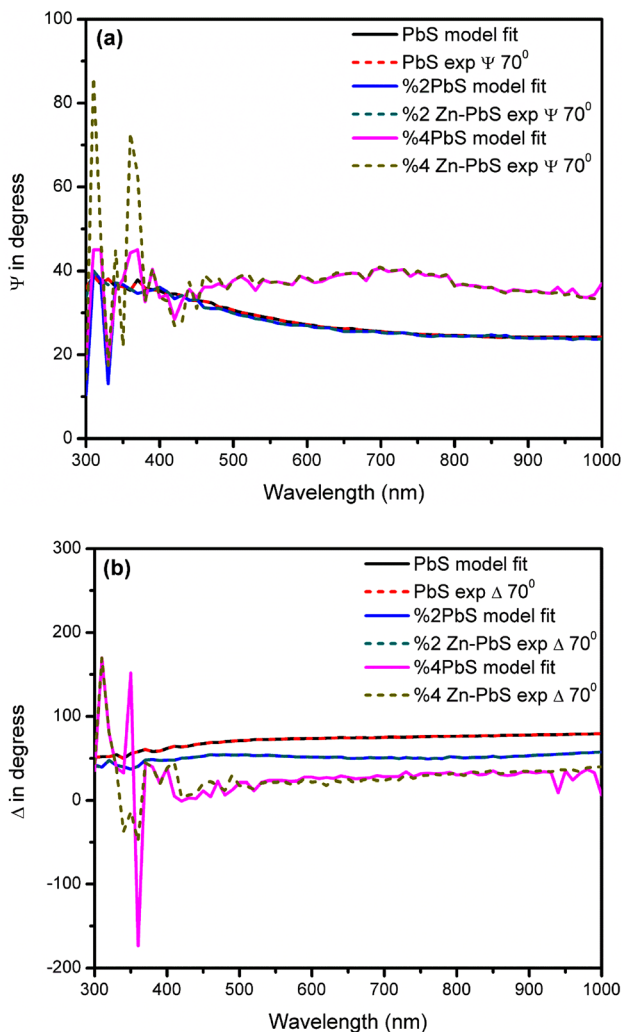


**Fig. 8** Model and fitting results of ellipsometric data of PbS films for **a** Psi ( $\Psi$ ), **b** Delta ( $\Delta$ )

When the refractive indices were searched, it was observed that the refractive indices values of Zn dopant decreased compared to the pure PbS thin film. This decrease in the value of the refractive index is due to the optical dispersion behavior of the material. It is also seen that the refractive indices of Zn-doped PbS films are slightly less than that of the pure PbS film. The reason for this may be that the presence of Zn element in the PbS structure reduced the polarization ability of the electrons. L. N. Ezenwaka et al. reported high value of the refractive index demonstrated by the films and they attributed it to the high absorbance of the films [40].

The extinction coefficient is related to the absorption property of the material, and is a measure of the portion of the beam lost as it passes through the medium. Radiation loss is a result of scattering and absorption per unit distance of the medium [41]. It can be seen from Fig. 10 that the values of the extinction coefficients varied between 0.75 and 1.2 for all semiconductor thin films, and they were in a suitable range for the absorber layer. Additionally, the Zn dopant caused a decrease in the extinction coefficient. B. Touati et al. reported that the values of extinction coefficients are slightly lower than in this study [42].

In general, the dielectric constants are highly contingent upon the electronic structure of the material and can be said to be exactly relevant to the state density in the band gap, which have an impact on the electromagnetic radiation passing through the material. The values imaginary and real and dielectric

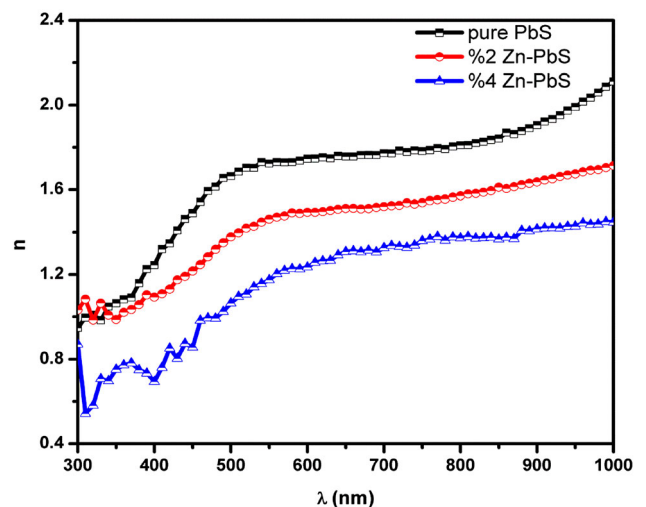


**Fig. 9** Changes of refractive index as a function of wavelength for pure and Zn-doped PbS

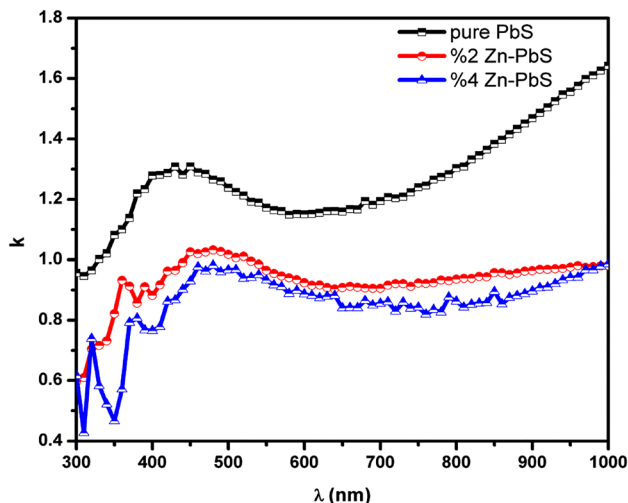


**Fig. 10** The graph of extinction coefficient of pure, 2%, and 4% Zn-doped PbS thin films

constants were determined using the following relations [43, 44]:

$$\epsilon_1 = n^2 - k^2 \quad (4)$$

$$\epsilon_2 = 2nk \quad (5)$$

In Figs. 11 and 12, it was seen that the imaginary and real dielectric constant values of pure and Zn-doped PbS thin films increased with the increase of wavelength and it was compatible with the refractive index graphs. Real dielectric constant values show a sharper increase in the wavelength range of 400–700 nm. It is also seen that, the Zn dopant caused a decrease in the dielectric constants. V. V. Jadhavar and B. S. Munde reported that the Cr-doped ZnS nanoparticles have a higher dielectric constant, which decreases as the Cr concentration increases [45]. In addition, when the graphs are examined, it is observed that the real and imaginary dielectric constant values for all nanostructured thin films vary significantly in the visible region. It is seen that the mean  $\epsilon_2$  values are higher than  $\epsilon_1$  in all samples. This difference between the real and imaginary parts is related to the state densities in the energy band gaps of the films. Similar observations are reported by references of [46] and [47].

The energy loss function has an important place in optoelectronic device applications. The total power loss (volume and surface energy) transferred across the dielectric is important. Dissipation factor ( $\tan(\delta)$ ) is a precious term in the reviewing of structure and defects in materials and also symbolizes the phase

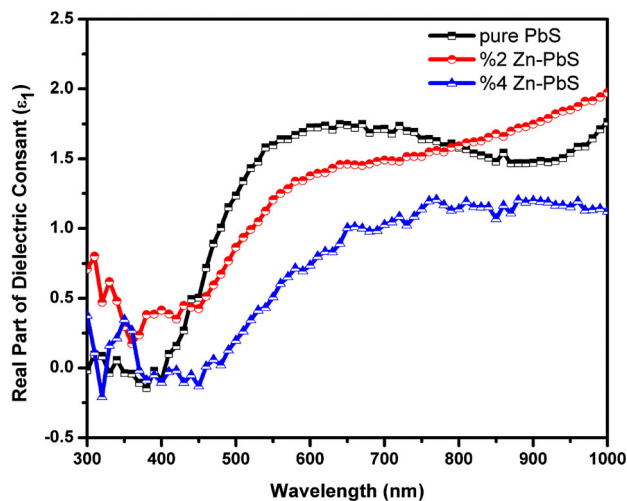


**Fig. 11** Changes of real part of dielectric constant as a function of wavelength for pure and Zn-doped PbS

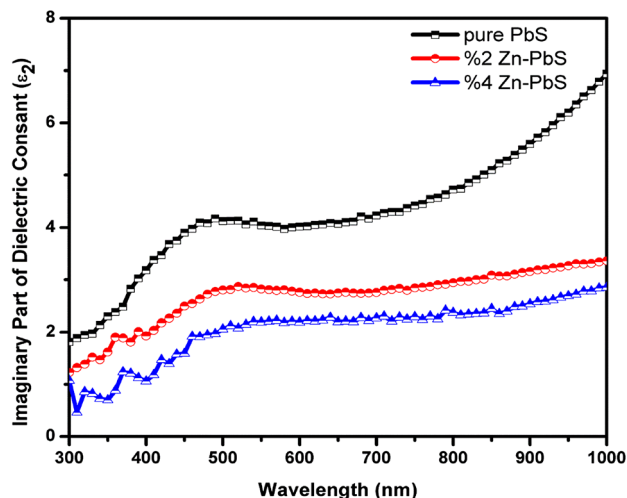


**Fig. 12** Changes of imaginary part dielectric constant as a function of wavelength for pure and Zn-doped PbS

difference in the materials due to energy loss. The perfection of the dielectric as an acceptable feature is characterized by low values of the dissipation factor. In a loss modulus system, the loss factor is related to the rate of loss of  $\tan \delta$  power.  $\tan(\delta)$  depends on the real and imaginary part of the dielectric constants as follows [48]:

$$\tan \delta = \frac{\epsilon_2}{\epsilon_1} \quad (6)$$

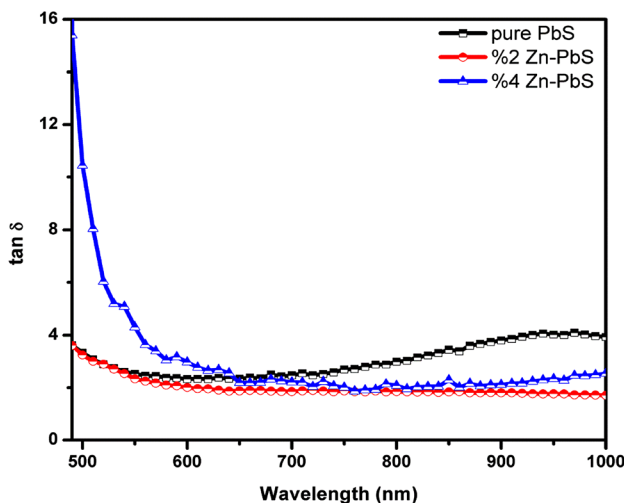
Here,  $\epsilon$  is the complex dielectric constant and comprises of real and imaginary parts  $\epsilon_1$  and  $\epsilon_2$ . (real  $\epsilon_1$ , imaginary  $\epsilon_2$ ).

Figure 13 shows the graph of wavelength versus  $\tan(\delta)$ . An almost constant dependence is observed for all wavelength values within the graph for pure and 2% Zn-doped PbS thin films and strong dependence is observed between 500 and 650 nm wavelength range for 4% Zn-doped PbS thin films. This is due to the sudden increase in the absorption coefficient. For Ge addition Pb–Se films, dielectric loss tangent showed higher values in the lower wavelength region (500–700 nm) for all samples in their investigations, and the energy losses decrease with the increase of Ge [49].

### 3.5 Dispersion parameters

The dispersion of optical parameters has an impact on materials research because of its importance in electro–optical device and communication. It is well known that the refractive index and hence the dielectric constant in any material changes with the photon energy and this change is described by dispersion expressions [50]. The variation of refractive index of many semiconductor materials with incident photon energy can be simply described with the help of the single-oscillator model proposed by Wemple–DiDomenico. This model is based on a fairly simple semi-empirical relation and is given as follows [51, 52]:

$$n^2(h\nu) = 1 + \frac{E_0 E_d}{E_0^2 - (h\nu)^2} \tag{7}$$



**Fig. 13** Dissipation factor vs. photon wavelength for pure, 2%, and 4% Zn-doped PbS thin films

Here,  $h$  is Planck’s constant;  $E_0$  is the single-oscillator energy,  $\nu$  is frequency, and  $E_d$  is the dispersion energy, which is defined as a measure of the average intensity of the optical transitions between the bands. The dispersion energy is basically a quantity nearly relevant to the charge distribution in the unit cell, and to chemical bonding. To determine the dispersion parameters  $E_0$  and  $E_d$  in the Wemple–DiDomenico model, the related equation can be arranged as follows [53]:

$$\frac{1}{n^2 - 1} = \frac{E_0^2 - (h\nu)^2}{E_d E_0} = \frac{E_0}{E_d} - \frac{(h\nu)^2}{E_d E_0} \tag{8}$$

In order to calculate the  $E_0$  and  $E_d$  values, firstly, the graph of the change of  $1/(n^2-1)$  with respect to  $(h\nu)^2$  was drawn in Fig. 14.

As expected from this graph, a linear region was obtained for all materials. The point where this linear curve intersects the vertical axis gives the ratio  $E_0/E_d$ , and its slope gives the value  $1/E_0 E_d$ . The  $E_0$  and  $E_d$  dispersion parameters for pure, 2%, and 4% Zn-doped PbS films from the calculations in the graph were found and tabulated in Table 2. In the Wemple–DiDomenico model, it is known that  $E_0$  is related to  $E_g$  and empirically changes to  $E_0 \approx 1.5 E_g$  for many materials. It has been observed that the  $E_0$  single-oscillator energy for pure PbS, 2%, and 4% Zn-doped PbS films is  $E_0 \approx 0.5 E_g$ . This relationship was obtained from the study conducted by A. S. Hasanien and A. A. Akl [54] and was found as almost equal to 2. For pure and Zn-doped CdO thin films,  $E_0$  and  $E_d$  dispersion parameters were found between

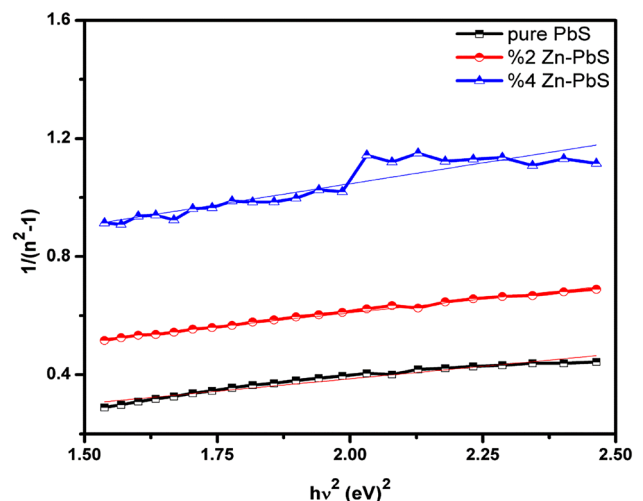


**Fig. 14** Plot of  $(n^2 - 1)^{-1}$  against  $(h\nu)^2$  for pure, 2%, and 4% Zn-doped PbS thin films

**Table 2** Calculated some optical values of the pure, %2, and %4 Zn-PbS thin films

Some optical values of PbS film samples	pure PbS	%2 Zn-PbS	%4 Zn-PbS
$E_g$ (eV)	1.95	1.99	2.07
$E_0$ (eV)	0.53	1.11	1.30
$E_d$ (eV)	11.08	4.77	2.71
$M_{-1}$	20.90	4.29	2.08
$M_{-3}$	74.40	3.48	1.23
$f$ (eV)	5.87	5.29	3.52

2.00 and 2.81 eV and 1.42–2.30 eV, respectively, in another study [55].

$$E_0^2 = \frac{M_{-1}}{M_{-3}} \quad (9)$$

and

$$E_d^2 = \frac{M_{-1}^3}{M_{-3}} \quad (10)$$

$M_{-1}$  and  $M_{-3}$  values for pure PbS, 2%, and 4% Zn-doped PbS films are calculated and tabulated in Table 2. These values are measures of the average bond strength. Optical moment values are related to the amount of macro coverage in the investigated materials, such as the effective dielectric constant and the number of effective valence electrons. A. M. Alsaad et al. reported that in ZnO thin films, as the boron concentration increases, the optical moment values increase, indicating that the B-doped thin films are highly polarized [56].

The optical oscillator power ( $f$ ) in optical transitions is the absorption of the photon by the electron during the transition. Oscillator power is a measure of how the optical material interacts with radiation, and  $f$  is given by the formula [57]:

$$f = E_0 \cdot E_d. \quad (11)$$

This value calculated for all semiconductor thin films is given in Table 2.

## 4 Conclusion

In this study, pure PbS and Zn-doped PbS films, whose value is increasing day by day in many optoelectronic and solar cell applications, were produced by electrodeposition method on ITO substrates. According to the XRD results used to determine the structural properties of the films, the

shifts in the distances between the diffraction angles and lattice planes of the films due to the ionic radius difference between the Zn element and the Pb element are evidence that the Zn element affects the structure. When the thickness values of the films determined by the spectroscopic ellipsometer device were examined, it was determined that they were close to each other. We think that these slight differences occur due to small deviations between theoretical and experimental delta values, which are equation parameters used during spectroscopic ellipsometer measurement. The optical properties of the films in this study, in three different devices, respectively, the absorption, transmittance, refractive index, and extinction coefficient values were taken against the wavelength. By using the absorption spectra and thickness values, the optical band gaps of the films were found from the graphs by optical method. In addition, it has been determined from these graphs that all of the films are direct bandpass films. When the optical transmittance spectra of pure, 2%, and 4% Zn-doped PbS semiconductor thin films were examined, it was determined that all Zn-doped thin film samples had better optical transmittance than the pure PbS sample. From the SEM images, it was determined that the films were properly coated on the substrates. As a result, considering the crystal structures, surface images, optical and dispersion properties of pure and Zn-doped-PbS semiconductor thin films, it can be said that they have a high potential to be used as layer materials in solar cells.

## Acknowledgements

This work was funded by Bilecik Seyh Edebali University Scientific Research Coordination Unit (Project Number: 2021-01.BŞEÜ.11 – 04).

## Author contributions

EE contributed to the design and implementation of the research, to the analysis of the results, and to the writing of the manuscript. AKY aided in interpreting the results. Both authors contributed to the final version of the manuscript.

## Data Availability

The data used to support the findings of this study are included within the article.

## Declarations

**Conflict of interest** The author declares that there is no conflict of interests regarding the publication of this paper.

## References

1. S.M. Sze, Y. Li, K.K. Ng, *Physics of Semiconductor Devices* (Wiley, New York, 2021)
2. A.D. Pogrebnyak, L.F. Sukhodub, L. Sukhodub, O.V. Bondar, A. Turlybekuly, *Advances in Thin Films, Nanostructured Materials, and Coatings* (Springer, Berlin, 2019)
3. K.M. Gupta, N. Gupta, Recent Advances in Semiconducting Materials and Devices. In *Advanced Semiconducting Materials and Devices*. (Springer, Cham, Springer International Publishing Switzerland, 2016), pp.531–562
4. M. Eslamian, Inorganic and organic solution-processed thin film devices. *Nano-micro Lett.* **9**(1), 1–23 (2017)
5. A.E. Madani, O. Daoudi, S. Benyoussef, A. Qachaou, M. Fahoume, M. Lharch, Experimental and ab initio investigation of the physical properties of PbS thin films prepared by chemical bath deposition (CBD). *Braz. J. Phys.* **51**(4), 1166–1174 (2021)
6. A. El madani, R. Essajai, A. Qachaou, A. Raidou, M. Fahoume, M. Lharch, The temperature effect on the physical properties of PbS thin films produced by the chemical bath deposition (CBD) technique. *Adv. Mater. Process. Tech.* **8**(3), 3413–3424 (2022)
7. E. Barrios-Salgado et al., Effect of deposition time on the optoelectronics properties of PbS thin films obtained by microwave-assisted chemical bath deposition. *Adv. Cond. Matter. Phys.* **2019**, 1–8 (2019)
8. R.M. Woo-García et al., Structure, morphology, and local photoelectrical characterization of PbS films grown by SILAR. *Mater. Lett.* **314**, 131844 (2022)
9. J.M.C. da Silva Filho, F.C. Marques, Structural and optical temperature-dependent properties of PbS thin films deposited by radio frequency sputtering. *Mater. Sci. Semicond. Process.* **91**, 188–193 (2019)
10. E. Sarica, V. Bilgin, Effect of pb: S molar ratio in precursor solution on the properties of lead sulphide thin films by ultrasonic spray pyrolysis. *Mater. Sci. Semicond. Process.* **71**, 42–49 (2017)
11. U. Chalapathi, S.H. Park, W.J. Choi, Chemically grown highly crystalline PbS thin films with ethylenediamine tetraacetic acid complexing agent. *Mater. Sci. Semicond. Process.* **134**, 106022 (2021)
12. I. Ikhioya, S. Ehika, B. Ijabor, Influence of deposition potential on lead sulphide (PbS) thin film using electrodeposition technique. *Asian J. Chem. Sci.* **3**(4), 1–8 (2018)
13. S. Ehika, I.L. Ikhioya, Effects of solution concentration of the optical and electrical properties of lead sulphide (PbS) semiconductor thin films deposited by electrodeposition technique. *Niger Ann. Nat. Sci.* **16**(1), 066–075 (2017)
14. E. Erdoğan, M. Yilmaz, S. Aydogan, G. Turgut, Investigation of neodymium rare earth element doping in spray-coated zinc oxide thin films. *J. Mater. Sci.: Mater. Electron.* **32**(2), 1379–1391 (2021)
15. K. Paulraj et al., Investigation of samarium-doped PbS thin films fabricated using nebulizer spray technique for photosensing applications. *Superlattices Microstruct.* **148**, 106723 (2020)
16. S.R. Rosario et al., Ag-doped PbS thin films by nebulizer spray pyrolysis for solar cells. *Int. J. Energy Res.* **44**(6), 4505–4515 (2020)
17. U. Chalapathi, S.H. Park, W.J. Choi, Chemically deposited Sn-doped PbS thin films for infrared photodetector applications. *Appl. Phys. A* **127**(9), 1–6 (2021)
18. K. Paulraj et al., Comprehensive study on nebulizer-spray-pyrolyzed Eu-Doped PbS thin films for optoelectronic applications. *J. Electron. Mater.* **49**(9), 5439–5448 (2020)
19. M.H. Jameel et al., A comparative study on characterizations and synthesis of pure lead sulfide (PbS) and Ag-doped PbS for photovoltaic applications. *Nanotechnol. Rev.* **10**(1), 1484–1492 (2021)
20. C. Sabitha, K.D.A. Kumar, S. Valanarasu, A. Saranya, I.H. Joe, Cu: ZnS and Al: ZnS thin films prepared on FTO substrate by nebulized spray pyrolysis technique. *J. Mater. Sci.: Mater. Electron.* **29**, 4612–4623 (2018)
21. E. Erdoğan, X-ray line-broadening study on sputtered InGaN semiconductor with evaluation of Williamson–Hall and size–strain plot methods. *Indian J. Phys.* **93**(10), 1313–1318 (2019)

22. A. Monshi, M.R. Foroughi, M.R. Monshi, Modified scherrer equation to estimate more accurately nano-crystallite size using XRD. *World. J. Nano Sci. Eng.* **2**, 154–160 (2012)
23. L.R. Singh, M.A. Hussain, Effect of doping concentration on the optical properties of nanocrystalline Zn Doped PbS thin films deposited by CBD method. *Chalcogenide Lett.* **17**(11), 583–591 (2020)
24. E.A. Abiodun et al., Surface microstructure, optical and electrical properties of spray pyrolyzed PbS and Zn-PbS thin films for optoelectronic applications. *Mater. Sci. -Pol.* **35**(3), 576–582 (2017)
25. M.A. Hussain, L.R. Singh, S.R. Devi, Studies on structural, optical and electrical properties of Zn-Doped PbS nanocrystalline thin film. *Chalcogenide Lett.* **18**(3), 103–111 (2021)
26. D.A. Boyd, Sulfur and its role in modern materials science. *Angew. Chem. Int. Ed.* **55**(50), 15486–15502 (2016)
27. E. Erdoğan, M. Kundakçı, Changes of the physical properties of sputtered InGaN thin films under small nitrogen gas flow variations. *J. Electron. Mater.* **48**(5), 2924–2931 (2019)
28. E. Veena, K.V. Bangera, G.K. Shivakumar, Study on structural, optical and electrical properties of spray pyrolysed  $Pb_xZn_{1-x}S$  thin films for opto-electronic applications. *Optik* **144**, 528–538 (2017)
29. M. Liu et al., Effect of Zn doping concentration on optical band gap of PbS thin films. *J. Alloys Compd.* **792**, 1000–1007 (2019)
30. A.E. Adeoye et al., Effects of Zn doping concentration on the optical and photovoltaic properties of  $Zn_xPb_{1-x}S$  thin film-based solar cell prepared by chemical spray pyrolysis. *SN Appl. Sci.* **2**(9), 1–10 (2020)
31. E. Erdoğan, G. Turgut, M. Yilmaz, Sol-gel spin coating derived cadmium oxide semiconductor thin films: Effect of lutetium contribution. *Optik* **240**, 166819 (2021)
32. S. Ravishankar, A.R. Balu, Studies on ternary PbZnS films suited for optoelectronic applications. *Surf. Eng.* **33**(7), 506–511 (2017)
33. E. Yücel, Y. Yücel, Fabrication and characterization of Sr-doped PbS thin films grown by CBD. *Ceram. Int.* **43**(1), 407–413 (2017)
34. F.G. Hone, F.B. Dejene, Synthesis and characterization of lead sulphide thin films from ethanolamine (ETA) complexing agent chemical bath. *Mater. Res. Express* **5**(2), 026409 (2018)
35. D.H. Yeon et al., Origin of the enhanced photovoltaic characteristics of PbS thin film solar cells processed at near room temperature. *J. Mater. Chem. A* **2**(47), 20112–20117 (2014)
36. A. Cantas, G. Aygun, R. Turan, Impact of incorporated oxygen quantity on optical, structural and dielectric properties of reactive magnetron sputter grown high- $\kappa$  HfO<sub>2</sub>/Hf/Si thin film. *Appl. Surf. Sci.* **318**, 199–205 (2014)
37. A. Cantas, G. Aygun, D.K. Basa, In-situ spectroscopic ellipsometry and structural study of HfO<sub>2</sub> thin films deposited by radio frequency magnetron sputtering. *J. Appl. Phys.* **116**(8), 083517 (2014)
38. A. Cantas et al., Importance of CdS buffer layer thickness on Cu<sub>2</sub>ZnSnS<sub>4</sub>-based solar cell efficiency. *J. Phys. D Appl. Phys.* **51**(27), 275501 (2018)
39. C. Aydin, The dispersion energy parameters, linear and nonlinear optical properties of transparent mn: ZnO nanolayers. *Eur. Mech. Sci.* **4**(2), 82–89 (2020)
40. L.N. Ezenwaka et al., Investigation of the optical, structural and compositional properties of electrodeposited lead manganese sulfide (PbMnS) thin films for possible device applications. *Nanoarchitectonics* **3**(1), 18–32 (2022)
41. H. Zaka et al., Investigation of dispersion parameters, dielectric properties and opto-electrical parameters of ZnO thin film grown by ALD. *Optik* **203**, 163 (2020)
42. B. Touati, A. Gassoumi, S. Alfaify, N. Kamoun-Turki, Optical, morphological and electrical studies of Zn: PbS thin films. *Mater. Sci. Semicond. Process.* **34**, 82–87 (2015)
43. I.M. El Radaf, I.H.Y.S. Al-Zahrani, A.S. Hassanien, Novel synthesis, structural, linear and nonlinear optical properties of p-type kesterite nanosized Cu<sub>2</sub>MnGeS<sub>4</sub> thin films. *J. Mater. Sci.: Mater. Electron.* **31**(11), 8336–8348 (2020)
44. Y. Bchiri, N. Bouguila, M. Kraini, S. Alaya, Annealed In<sub>2</sub>S<sub>3</sub> thin Films prepared by spray technique: report on the Structural, Optical and Dispersion Energy Parameters. *Surf. Rev. Lett.* **26**(07), 1850223 (2019)
45. V.V. Jadhavar, B.S. Munde, Investigation of structural, optical, and dielectric properties of Zn<sub>1-x</sub>CrxS nanoparticles for optoelectronic applications. *J. Mater. Sci.: Mater. Electron.* **33**(30), 23867–23877 (2022)
46. A. Goktas, F. Aslan, A. Tumbul, S.H. Gunduz, Tuning of structural, optical and dielectric constants by various transition metal doping in ZnO: TM (TM = Mn, Co, Fe) nanostructured thin films: a comparative study. *Ceram. Int.* **43**(1), 704–713 (2017)
47. K. Paulraj et al., Praseodymium doped PbS thin films for optoelectronic applications prepared by nebulizer spray pyrolysis. *Appl. Phys. A* **126**(7), 1–10 (2020)
48. E. Erdogan, Coronene organic films: optical and spectral characteristics under annealing temperature influences. *Surf. Rev. Lett.* **28**(09), 2150081 (2021)
49. A.S. Hassanien, I. Sharma, Dielectric properties, optoelectrical parameters and electronic polarizability of thermally evaporated a-pb-se-ge thin films. *Phys. B Condens. Matter* **622**, 413330 (2021)
50. H.A.M. Ali et al., Optical and dispersion properties of thermally deposited phenol red thin films. *Opt. Laser Technol.* **107**, 402–407 (2018)

51. S.H. Wemple, DiDomenico behavior of the electronic dielectric constant in covalent and ionic materials. *Phys. Rev. B* **3**(4), 1338 (1971)
52. S.H. Wemple, Refractive-index behavior of amorphous semiconductors and glasses. *Phys. Rev. B* **7**(8), 3767 (1973)
53. H.S. Wasly et al., Morphological, structural, and optical properties of flexible tin oxide (II) thin film via thermal evaporation technique. *Eur. Phys. J. Plus* **137**(1), 1–10 (2022)
54. A.S. Hassanien, A.A. Akl, Optical characterizations and refractive index dispersion parameters of annealed TiO<sub>2</sub> thin films synthesized by RF-sputtering technique at different flow rates of the reactive oxygen gas. *Phys. B Condens. Matter* **576**, 411718 (2020)
55. S.S. Yahia et al., Linear and nonlinear optical discussions of nanostructured Zn-doped CdO thin films. *Phys. B Condens. Matter* **511**, 54–60 (2017)
56. A.M. Alsaad et al., Optical band gap and refractive index dispersion parameters of boron-doped ZnO thin films: a novel derived mathematical model from the experimental transmission spectra. *Optik* **211**, 164641 (2020)
57. D. Sahoo et al., Optimization of linear and nonlinear optical parameters of As<sub>40</sub>Se<sub>50</sub>Te<sub>10</sub> thin films by thermal annealing. *Opt. Laser Technol.* **140**, 107036 (2021)

**Publisher's note** Springer Nature remains neutral with regard to jurisdictional claims in published maps and institutional affiliations.

Springer Nature or its licensor (e.g. a society or other partner) holds exclusive rights to this article under a publishing agreement with the author(s) or other rightsholder(s); author self-archiving of the accepted manuscript version of this article is solely governed by the terms of such publishing agreement and applicable law.